CAMBRIDGE
UNIVERSITY PRESS

RESEARCH ARTICLE

Design, modeling, and control of a novel soft-rigid knee joint robot for assisting motion

Yinan Li[1], Yuxuan Wang[1] , Shaoke Yuan[1] and Yanqiong Fei[2]

[1]Research Institute of Robotics, Shanghai Jiao Tong University, Shanghai, 200240, China and [2]Research Institute of Robotics, Shenzhen Research Institute, Institute of Medical Robotics, Shanghai Jiao Tong University, Shanghai, 200240, China
Corresponding author: Yanqiong Fei; Email: fyq_sjtu@163.com

Abstract

This paper presents the design, modeling, and control of a novel soft-rigid knee joint robot (SR-KR) for assisting motion. SR-KR is proposed to assist patients with knee joint injuries conducting gait training and completing walking movements. SR-KR consists of a novel soft-rigid bidirectional curl actuator, a thigh clamping structure, and a crus clamping structure. The actuating part of SR-KR is composed of soft materials, which ensures the wearing comfort and safety, while the wearing parts contain rigid structure, which ensures the efficient transmission of torque. The bending deformation model of SR-KR is established, which reveal the relationship among SR-KR's bending curvature, working pressure, and output torque. Experiments show that SR-KR can provide more than 26.3 Nm torque for knee joint motion in human gait range. A double closed loop servo control system including attitude servo and pressure servo is built to better apply SR-KR. Mechanical property test, trajectory-driven test, and lower limb wearing test have been conducted, which show that SR-KR has ability to assist in lower limb motion and has potential in the fields of rehabilitation and human enhancement.

1. Introduction

In recent years, wearable robot has become a hot topic in academic and commercial fields [1–3]. Wearable robot means a robot that can extend, complement, substitute, or enhance human function and capability [4, 5]. As one of the largest and most complex joints in the human body [6], knee joint is very vulnerable to injuries or diseases such as arthritis [7, 8]. Such injuries to the knee joint greatly affect the daily lives of patients, who often need others' help or tools such as crutches to walk. Therefore, knee joint wearable robot for assisting motion has received widespread attention [9].

In the early development stage, a large number of pure rigid knee wearable robots have been proposed [10, 11]. These robots provide joint torque through hydraulic devices or motors. They apply torque to human body through rigid connecting rods for assisting motion [9]. Such robots have the advantages of mature manufacturing method, high operating accuracy, high torque transmission efficiency, and large output torque [12]. However, they also face problems such as poor fit with the human body, the rotation center cannot match the human joint rotation axis well, and large weight [13, 14] .

Recently, soft robotics has been gradually applied to the field of wearable robots because of their low weight, large deformation, lost cost, and good adaptivity to human body [15–17]. The soft wearable robot is mainly divided into two types: tendon-driven mode [18] and bending-driven mode [19].

Tendon-driven soft wearable robot uses soft materials as artificial tendons to assist human movements by stretching the user's limbs [18]. Common soft materials of these robots include cables, ropes, memory alloys, and other materials [18, 20]. Such robots have the advantages of light weight and long service life [21, 22]. However, because the force of such robots will act on the user's limb along with the artificial

Table I. *Key features of the state-of-the-art in soft wearable robots.*

Device	Assisting joints	Max continuous torque (Nm)	Range of motion (°)	Wearing position
Soft elbow exosuit [23]	Elbow	27.6	107	Outer side of the joint
Novel accordion-inspired foldable pneumatic actuators [24]	Knee	25.7	360	Inner side of the joint
Soft, wearable, and pleated pneumatic interference actuator [3]	Knee	324	86.7	Inner side of the joint
Soft-inflatable Exosuit [25]	Knee	4.4	>60	Inner side of the joint
Unfolding textile-based pneumatic actuators [26]	Shoulder	74.9	180	Inner side of the joint
Modular soft-rigid pneumatic lower limb exoskeleton (knee part) [27]	Knee	5	126	Parallel side of the joint
Low-resistance, high-force and large-ROM fabric-based soft elbow exosuits [28]	Elbow	>5	130	Outer side of the joint
ExoBoot [29]	Ankle	39	60	Inner side of the joint
Soft-inflatable exosuit [30]	Knee	4.09	120°	Parallel side of the joint

tendon, which means that its force direction cannot be perpendicular to the limb, it will exert shear force on the limb. Therefore, tendon-driven wearable robot faces the challenge of safety and comfort.

Bending-driven soft wearable robot generates torque to assist human motion through bending of its soft actuator [19]. The force of such robots is perpendicularly applied to the human body on both sides of the actuator without shear force, and the soft part of the actuator can better adapt to the human joint axis. Therefore, these robots are more suitable to apply in wearable robot. Some research has been appeared in this filed in recent years.

Table I summarizes the assisting joints, max continuous torque, range of motion, and wearing position of a number of bending-driven soft wearable robot in recent. These soft wearable robots cover common joints in this field, such as knees, elbows, ankles, etc. Many robots can already provide users with considerable torque support and range motion.

However, for wearable robots, there are three wearing positions: outer side of the joint, inner side of the joint, and parallel side of the joint, as shown in Fig. 1. From Fig. 1, it can be noted that wearing on the outer side of the joint or inner side of the joint cannot align the robot's rotation axis with the human joints, so this may generate shear force on the human joints during the assisting process, affecting the safety and wearing comfort of the robot. Among the robots in Table I, only modular soft-rigid pneumatic lower limb exoskeleton (knee part) [27] and soft-inflatable exosuit [30] are worn on the parallel side of the joint, but the torque provided by both is relatively small, only 5 Nm and 4.09 Nm. Besides, most of these soft wearable robots face challenges of complex structures and cumbersome production, and the wearing with human body is also quite troublesome.

Based on the above, this research combines the advantages of rigid robot and soft robot to propose a novel soft-rigid knee joint robot (SR-KR) for assisting motion, which is equipped with soft bending
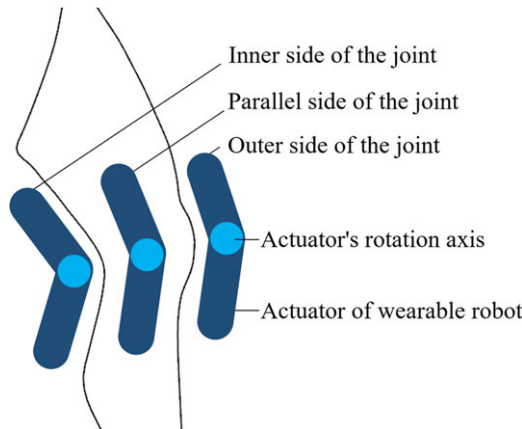
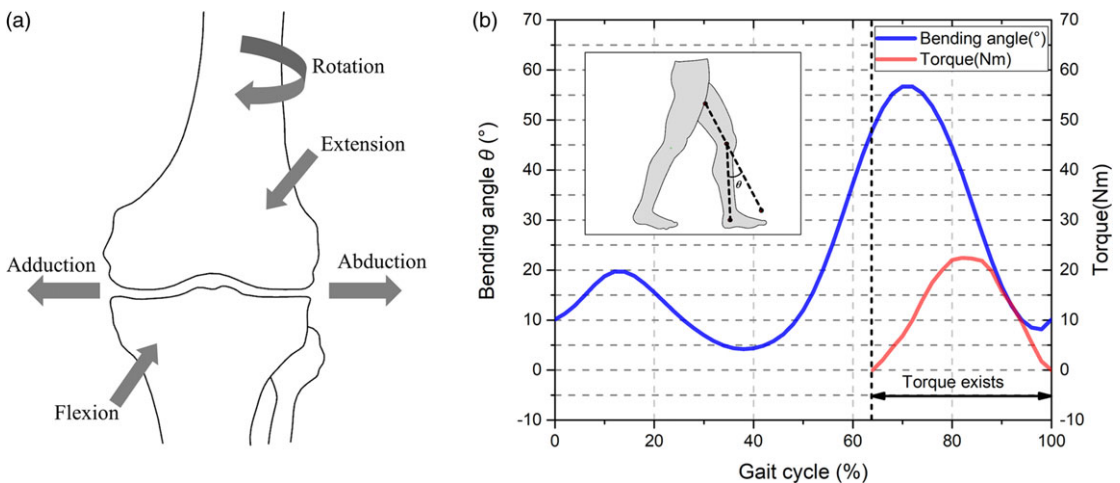**Figure 1.** *Wearing positions of wearable robots.*

Figure 2. *Ergonomic design. (a) Knee joint degrees of freedom. (b) Knee bending angle and torque in human gait range.*

part and rigid force transmission part. SR-KR is worn on the parallel side of the knee joint and provides the torque and range of motion of the knee joint under human gait range, which fills the gap in this field and promoting the development of wearable robots.

This paper is organized into six sections: Introduction, Design, Modeling, Control, Test, and Conclusions.

2. Design

2.1. Ergonomic design

From the perspective of ergonomics, knee joint movements include rotation, extension/flexion, and adduction/abduction, as shown in Fig. 2a. In the process of human walking, the main action is sagittal extension/flexion of the knee joint. Rotation and adduction/abduction degrees of freedom are mainly used to ensure the coordination, balance, and efficiency of human walking. Therefore, SR-KR will actively provide torque for extension/flexion degree of freedom. The other degrees of freedom will passively cooperate with the knee joint through the SR-KR soft actuating part. The purpose of this design is to reduce the complexity and weight of SR-KR, while ensuring its safety and comfort.
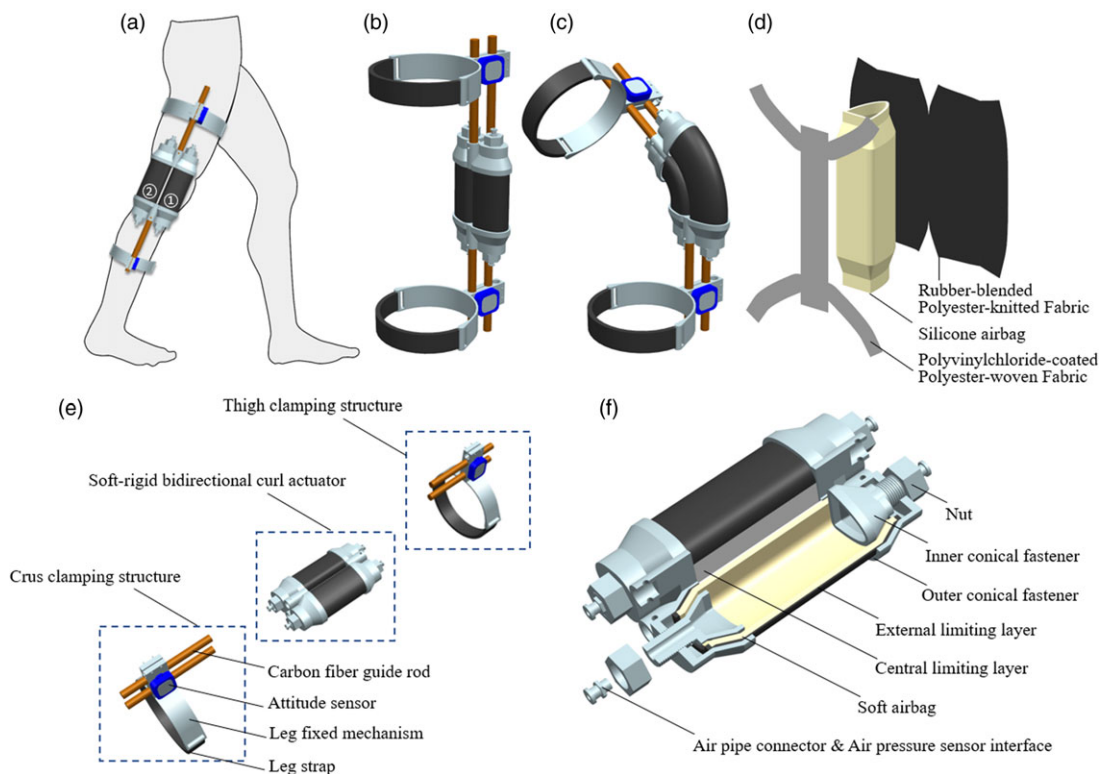
Figure 3. *Structure design of the SR-KR. (a) The wearing concept. (b) Appearance of SR-KR. (c) Bending deformation of SR-KR. (d) Components of air chamber. (e) Components of SR-KR. (f) Structure of the novel soft-rigid bidirectional curl actuator.*

In order to further determine the functional requirements of SR-KR, literature survey was conducted on the gait of knee joint. The relationship between knee joint bending angle (extension/flexion) and required torque under human gait range is shown in Fig. 2b [25, 31]. It can be noted that in a human gait cycle, the maximum bending angle of the knee joint is approximately 56.7°, and the maximum torque required is approximately 22 Nm. This result is also consistent with the researches of Takenagura et al. [32] and Nordez et al. [33]. Therefore, we get two functional requirements of SR-KR:

1. SR-KR can continuously carry out more than 56.7° load bending motion.
2. The output torque of SR-KR should be greater than 22 Nm.

2.2. Structure design

The overall structure of SR-KR is shown in Fig. 3, which is mainly composed of a novel soft-rigid bidirectional curl actuator, a thigh clamping structure, and a crus clamping structure (Fig. 3e). They are fixed by screws and nuts.

The design concept of the soft-rigid bidirectional curl actuator is pressure driving, airbag expansion, fabric limiting, and bending deformation. The main body of the actuator is two symmetrically distributed soft air chambers. Each air chamber is composed of a soft airbag, a central limiting layer, and an external limiting layer. These three parts are tightly pressed and fixed by screws and nuts at both ends of the chamber through matching conical fasteners (Fig. 3f).

The soft airbag is made of silicone material (ELASTOSILM 4601 A/B), and its main task is expanding under pressure. The section shape of soft airbag is semi-elliptical, which is convenient for axial

bending deformation. The central limiting layer is made of non-tensile material, polyvinylchloride-coated polyester-woven fabric to limit the deformation of the soft airbag's plane side. The external limiting layer is made of rubber-blended polyester-knitted fabric, which can be only one-way deformed. The external limiting layer limits the radial deformation of the soft airbag's curved side. These two limiting layers are formed by laser cutting. They are stitched at edges and combined to tightly wrap the soft airbag, so that the soft airbag can only undergo axial bending deformation. The conical fastener is made of aluminium alloy materials.

The design of conical fasteners removes the boundary lines that are easily damaged in traditional air chambers. Therefore, SR-KR has the advantage of high working pressure. Experiment shows that the actuator can withstand exceeding 400 kpa pressure. The conical fasteners are equipped with air pipe connector and pressure sensor interface to facilitate subsequent control work.

The thigh and crus clamping structure consist of carbon fiber guide rod, leg fixed mechanism, leg strap, and attitude sensor (Fig. 3e). The leg fixed mechanism is made of PLA materials by 3D printing and is fixed on the carbon fiber guide rod by screws and nuts. The leg fixed mechanism can move the installation position along the guide rod. Therefore, SR-KR can match people with different statures. The leg strap is connected to the leg fixed mechanism and can be adjusted by velcro. The attitude sensor is fixed on the leg fixed mechanism to detect the bending angle of SR-KR. The thigh and crus clamping structure is the wearing part of SR-KR, which is responsible for fixing SR-KR on human body.

When users need to use SR-KR to complete passive training, they can inflate the SR-KR air chamber near the front of their body (chamber 1 in Fig. 3a), while the other air chamber does not inflate or bleed. At this time, the SR-KR will generate the torque to help the users complete the knee joint bending motion. When users need to use SR-KR for impedance training, they can inflate the SR-KR air chamber near the back of their body (chamber 2 in Fig. 3a), while the other air chamber does not inflate. So, SR-KR will generate torque in the opposite direction of knee joint movement to help users complete knee joint impedance training.

The design idea of the SR-KR's structure is soft-rigid integration. SR-KR's bending deformation part contacted to knee is completely made of soft materials, which aims to ensure the good axis adaptivity and wearing safety. The force transmission part of SR-KR are rigid structures, which aims to ensure the efficient transmission of output torque.

2.3. Parameter design

The simplified lower limb connecting rod diagram is shown in Fig. 4a. The four connecting rods from top to bottom represent the waist, thigh, crus, and foot, respectively. The hollow circle represents the joint of each part. m_w, m_t, and m_c represent the centroids of each part. d_w, d_t, and d_c represent the length from the centroid of the relative part to the previous joint.

The size of SR-KR should be determined according to each user's actual lower limb size. Considering the wearing space of SR-KR, the whole length of SR-KR L_{whole} should be longer than the distance between the centroids of thigh and crus and shorter than the total length of thigh and calf as (1). The length of SR-KR's soft part l_{soft} should cover the whole knee l_{knee} but less than the length from the thigh centroid to the crus centroid as (2). The adaptable length of the thigh clamping structure $L_{\text{ad\_thigh}}$ should be longer than the length from the centroid of the thigh to the hip joint, and less than the thigh length as (3). Similarly, the adaptable length of the crus clamping structure $L_{\text{ad\_crus}}$ should be longer than the length from the centroid of the crus to the ankle joint and less than the crus length as (4). Considering of wearing comfort, the maximum thickness of SR-KR w_d should be less than the thickness of the user's knee joint as (5).

$$L_t - d_t + d_c \leq L_{\text{whole}} \leq L_t + L_c \tag{1}$$

$$l_{\text{knee}} < l_{\text{soft}} \leq L_t - d_t + d_c \tag{2}$$

$$d_t \leq L_{\text{ad}_{\text{thigh}}} \leq L_t \tag{3}$$

Table II. *Prototype parameters.*

| Parameter	Symbol	Value
Whole length of SR-KR	L_{whole}	565 mm
Soft air chamber length	L_{soft}	145 mm
Length of the soft-rigid bidirectional curl actuator	L_b	165 mm
Adjustable length of thigh clamping structure	$L_{\text{ad\_thigh}}$	70 mm
Adjustable length of crus clamping structure	$L_{\text{ad\_crus}}$	55 mm
Matching length of SR-KR	L_{adjust}	425 mm–550 mm
Sectional area of soft chamber	A_{soft}	1919.38 mm^2
Maximum width of SR-KR	w_d	51 mm
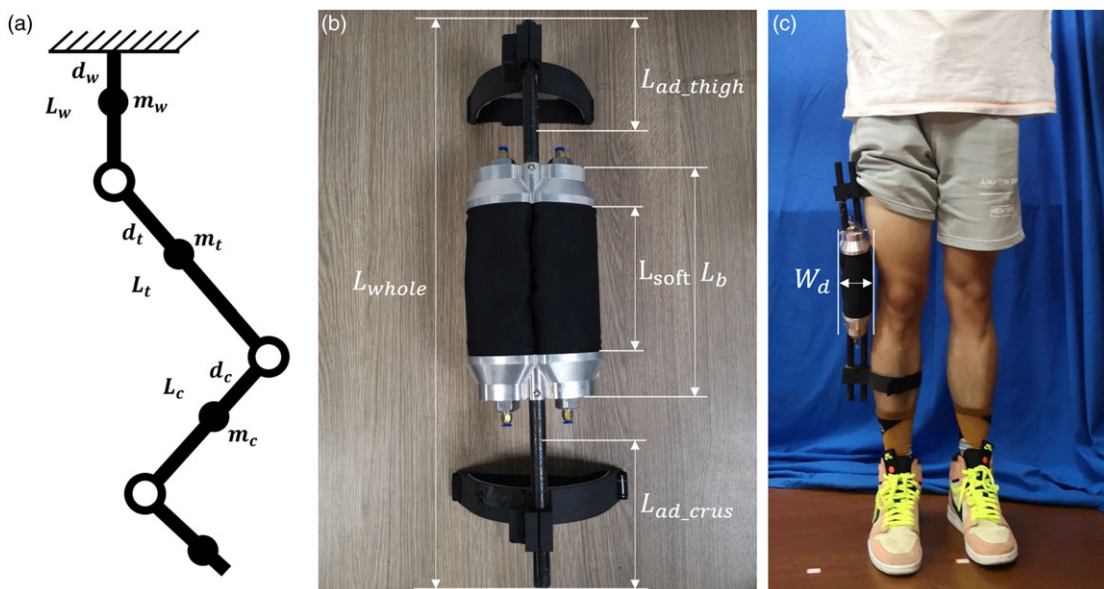
Figure 4. *Parameter design of SR-KR. (a) The simplified lower limb connecting rod diagram. (b) Parameters of the SR-KR. (c) Wearing diagram of SR-KR.*

$$L_c - d_c \leq L_{\text{ad}_{\text{crus}}} \leq L_c \tag{4}$$

$$w_d \leq w_{\text{knee}} \tag{5}$$

In this paper, we choose a 24-year-old male as the prototype user of SR-KR. This man is 178 cm tall and weighs 71 kg. Through the above analysis, we get the prototype parameters, as shown in Table II. The wearing diagram of SR-KR prototype is shown in Fig. 4c.

3. Modeling

3.1. Bending model of the actuator

When the air chamber at one side is inflated, the actuator will bend, as shown in Fig. 5a. The cross-section of the air chamber at this time is shown in Fig. 5b, which includes the central limiting layer, external limiting layer, soft airbag, and air chamber cavity.

Because of the material properties, the central limiting layer is not subject to tensile deformation, so it can be regarded as the bending neutral layer. The external limiting layer can only stretch and deform in
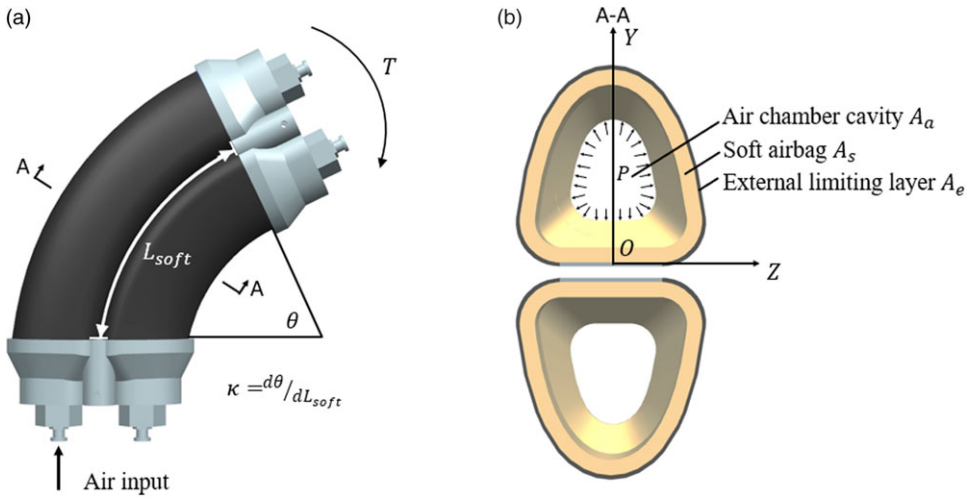
Figure 5. *Inflation bending diagram of SR-KR. (a) SR-KR's bending front view. (b) Section A-A of the SR-KR in (a).*

radial direction, which can restrain the expansion of the soft airbag in axial direction. Therefore, it can be approximately considered that the sectional shape of the soft air chamber remains unchanged during the bending process. So, we can establish the YOZ coordinate system as shown in Fig. 5b. The origin O of the coordinate system is the midpoint of the neutral layer, and the Z axis direction is parallel to the neutral layer.

When the actuator is inflated and bent, the moment on its section includes the external limiting layer moment M_e, the soft airbag moment M_s, the pressure moment M_p, and the possible output torque T. We can list the mechanical equation of the relative neutral layer when the bending is balanced, as shown in (6).

$$M_e + M_s - M_p + T = 0 \qquad (6)$$

Setting the sectional area of the external limiting layer, soft airbag, and air chamber cavity as A_e, A_s, and A_a, we can derive each item in (6) separately, as shown in (7)–(9).

$$M_e = \iint_{A_e} \sigma_e\left(\varepsilon\right) y dA \qquad (7)$$

$$M_s = \iint_{A_s} \sigma_s\left(\varepsilon\right) y dA \qquad (8)$$

$$M_p = \iint_{A_a} P y dA \qquad (9)$$

where $\sigma_e(\varepsilon)$, $\sigma_s(\varepsilon)$, and P are the axial tensile stress of the external limiting layer, the axial tensile stress of the soft airbag, and the working pressure of the actuator respectively.

Since the pressure in the air chamber cavity is consistent everywhere, we can simplify the pressure term as (10).

$$\iint_{A_a} P y dA = \iint_{A_a} y dA \cdot P = S_c P \qquad (10)$$

where, S_c is the static moment of the air chamber cavity.

The axial tensile stress of the external limiting layer and the soft airbag can be expressed as functions of their axial strain, ε. For soft materials, the stress-strain relationship is usually nonlinear. In this paper,

Table III.   Material parameters of the SR-KR.

Parameter	Symbol	Value (MPa)
Material parameters of soft airbag	E_{s0}	0.3849
	E_{s1}	−0.03262
	E_{s2}	0.0542
Material parameters of external limiting layer	E_{e0}	0.5784
	E_{e1}	−0.8632
	E_{e2}	0.7089

we select cubic function to fit the relationship, as shown in (11) and (12).

$$\sigma_e(\varepsilon) = E_{e0}\varepsilon + E_{e1}\varepsilon^2 + E_{e2}\varepsilon^3 \tag{11}$$

$$\sigma_s(\varepsilon) = E_{s0}\varepsilon + E_{s1}\varepsilon^2 + E_{s2}\varepsilon^3 \tag{12}$$

$E_e^{(i)}$ and $E_s^{(i)}$ ($i = 0, 1, 2$) are obtained through experiments and listed in Table III. ε is the axial strain of the soft airbag and the external limiting layer at each point of their cross-section. ε can be expressed by the bending curvature at the cross-section κ and the distance between the point and the neutral layer y, as shown in (13). Furthermore, since the cross-section of the soft chamber is same everywhere, it can be considered that the curvature κ of each cross-section is const.

$$\varepsilon = \kappa y \tag{13}$$

By substituting (7)–(13) into (6), we can get the relationship between the bending curvature, working pressure, and output torque of SR-KR, as shown in (14) and (15), where C_i are consts determined by material properties and section shape.

$$\left(C_0\kappa + C_1\kappa^2 + C_2\kappa^3\right) - S_c P + T = 0 \tag{14}$$

$$C_i = E_{ei}\iint_{A_e} y^{i+2}dA + E_{si}\iint_{A_s} y^{i+2}dA \tag{15}$$

Therefore, we can get the conclusions as below:

1. When the bending curvature of SR-KR is constant, the relationship between the output torque and the working pressure is linear. The proportional coefficient is the static moment of the air chamber cavity, which is only related to the section parameters of the air chamber.
2. When the working pressure is constant, the output torque of SR-KR is polynomial with its bending curvature. Polynomial coefficients are determined by section parameters and material properties.
3. When the output torque is constant, the working pressure is polynomial with its bending curvature. The polynomial coefficient is C_i/S_c, ($i = 0, 1, 2$).

3.2. Stiffness analysis of the actuator

The stiffness of a structure represents its ability to maintain shape under external loads [34]. In this paper, the actuator stiffness K is defined as the partial derivative of the actuator's bearing moment to its bending curvature, as shown in (16). The actuator's bearing moment means the moment acting on it, which is the opposite number of the actuator's output torque.

$$K = \frac{-\partial T}{\partial \kappa} = C_0 + C_1\kappa + C_2\kappa^2 \tag{16}$$
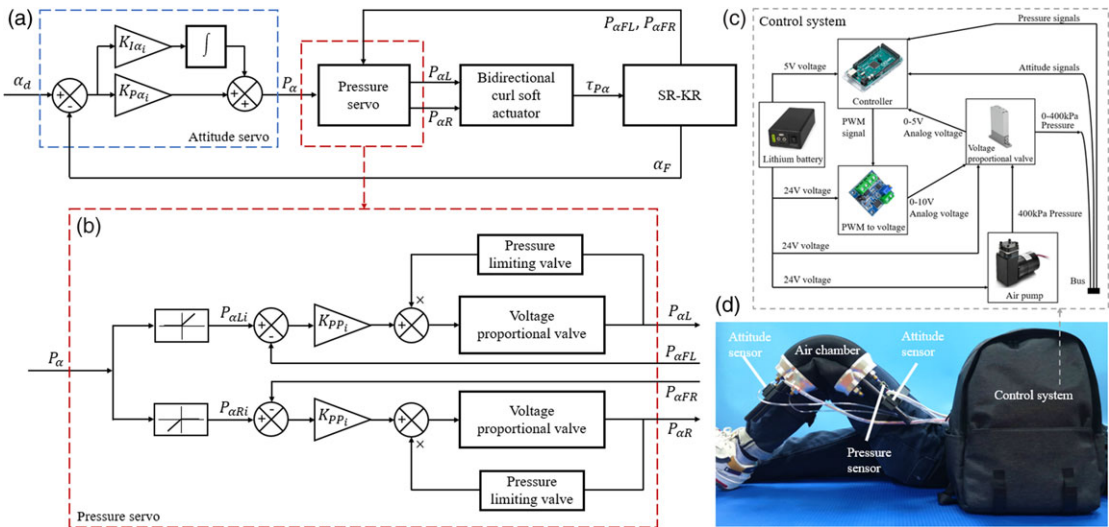
Figure 6. *Control system of SR-KR. (a) The double closed loop servo control system. (b) Pressure servo. (c) Composition of the system. (d) Integration of control system and SR-KR.*

From the (16), we can know:

1. The stiffness of the actuator is a quadratic function of its bending curvature. The stiffness of the actuator decreases first and then increases with the increase of curvature. This helps us to better use SR-KR.

2. When the bending curvature is constant, the stiffness of the actuator is only related to the material properties and the cross-section shape. So, the stiffness of actuator can be changed by changing these two terms.

4. Control

4.1. Double closed loop servo control system

In order to control and apply SR-KR more conveniently and safely, a double closed loop servo control system is built as shown in Fig. 6. This system consists of attitude servo and pressure servo. The two servos are independent of each other and work independently through their own feedback signals to achieve accurate control of SR-KR. The double closed loop structure of the system ensures the stability and safety of its operation, because every output will be double tested.

The pressure information of SR-KR is collected by the pressure sensor (XGZP6847500KPG; CFSensor) which can be equipped with the pressure sensor interface of SR-KR. The attitude information is obtained through the cooperation of the attitude sensors (WT901C TTL 9 Axis IMU Sensor; WitMotion) on the thigh and crus clamping structures.

Apart from these two sensors, the system also includes control board (Arduino Mega 2560), voltage proportional valve (SMC ITV0010 ITV0030 ITV0050-0/1/2/3BCLNS), PWM to voltage module, small air pump (ARP12DC24; 8bar; 17L/min; TIDE SMART TECHNOLOGY (SHANGHAI) CO., LTD, China), and lithium battery (YSN-37044800, YISENNENG). All the above components are integrated into a 42 cm × 32 cm × 12 cm backpack. The signal transmission relationship between the components is shown in Fig. 6c.

4.2. Attitude servo

For this paper, the attitude also means the bending angle α of SR-KR (Fig. 7). The attitude sensor chip selected is MPU9250, which can output quaternion, q_0, q_1, q_2, and q_3 after being calibrated by ellipsoid
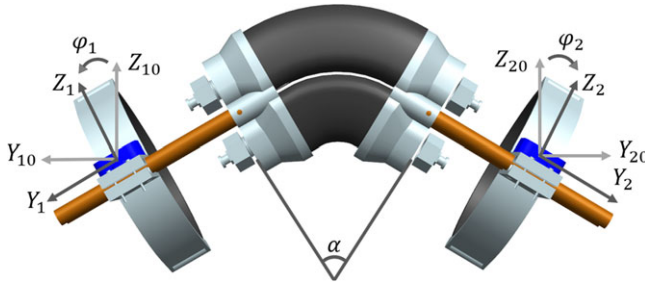
Figure 7. *Attitude change of MPU9250s during SR-KR bending.*

fitting method [35], as shown in (17). Through the operation between quaternions, we can obtain the spatial attitude of MPU9250. In this paper, by mirroring the placement of two MPU9250s at both ends (Fig. 8), the bending angle of SR-KR is the sum of the two sensors' rolling angle (φ_1, φ_2). Thus, the bending angle of SR-KR α can be obtained, as shown in (18) and (19).

$$q = q_0 + q_1 i + q_2 j + q_3 k \tag{17}$$

$$\varphi = \arctan \frac{2 \left(q_0 q_1 + q_2 q_3\right)}{1 - 2 \left(q_1{}^2 + q_2{}^2\right)} \tag{18}$$

$$\alpha = \varphi_1 + \varphi_2 \tag{19}$$

The attitude error is obtained from the difference between the input attitude preset signal α_d and the attitude feedback signal α_F. The error is processed by proportional gain $K_{P\alpha_i}$ and integral gain $K_{I\alpha_i}$ to obtain the preset pressure value. The proportional gain is added to speed up the response of the system, while the integral gain coefficient is added to eliminate the steady-state error and make the system more stable and accurate.

4.3. Pressure servo

In the pressure servo (Fig. 6b), the control of SR-KR's left and right air chambers is independent. First, when the preset pressure signal P_α is input, the pressure servo will filter it as shown in (20) to ensure that the pressure is distributed to the correct chamber. Then, the error is obtained by calculating the difference between the preset pressure signal ($P_{\alpha Li}$, $P_{\alpha Ri}$) and the pressure feedback signal ($P_{\alpha FL}$, $P_{\alpha FR}$). Next, the error will be amplified by the proportional gain (K_{PP_i}) to obtain the left and right voltage proportional valve signal (0-10V). Finally, the voltage proportional valve releases the corresponding pressure to actuate SR-KR.

$$\begin{cases} P_{\alpha Li} = P_\alpha, \text{ if } P_\alpha \geq 0 \\ P_{\alpha Ri} = P_\alpha, \text{ if } P_\alpha < 0 \end{cases} \tag{20}$$

Since the control board cannot directly output 0–10 V voltage signal, PWM wave signal is selected as the control signal of pressure intensity. The PWM signal is transmitted to the voltage proportional valve through the PWM to voltage module. At the fixed frequency, the output pressure of the proportional valve has a linear relationship with the duty cycle (21).

$$P = \beta P_0 \tag{21}$$

where P is the output pressure of the proportional valve, β is the duty cycle of PWM wave, and P_0 is the input pressure of the proportional valve.
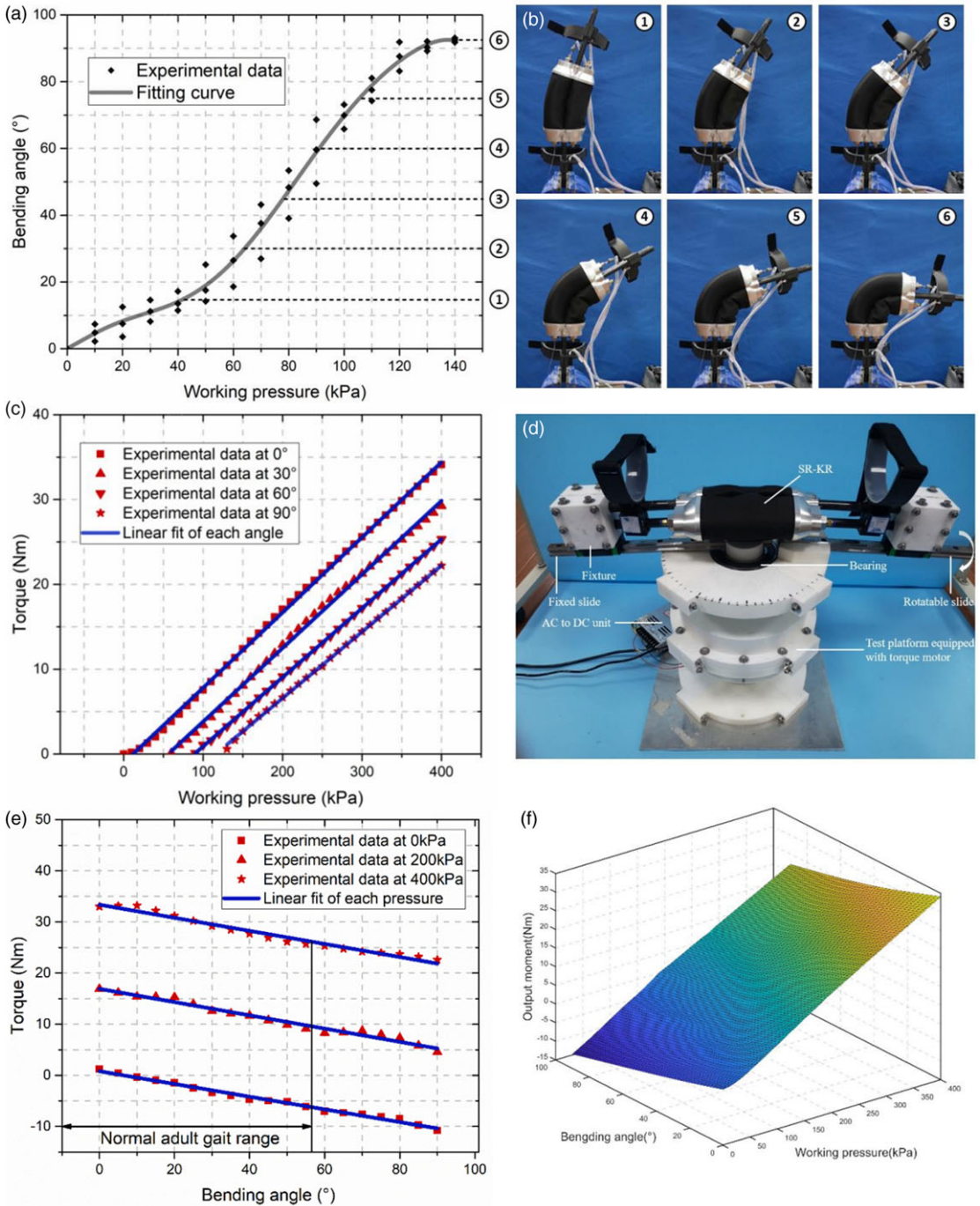
Figure 8. *Mechanical property test of SR-KR. (a) Free bending test. (b) Motion attitude of SR-KR at the corresponding points. (c) Constant bending angle test. (d) Torque test platform. (e) Constant working pressure test. (f) Relational surface for bending angle, working pressure, and output torque for SR-KR.*

For the safe use of SR-KR, the pressure limiting value is set in the pressure servo. When the pressure feedback signal ($P_{\alpha FL}$, $P_{\alpha FR}$) is greater than 400 kPa, the voltage proportional valve signal will be multiplied by 0, that is, it will stop working.

5. Test

5.1. Free bending test

In order to evaluate the bending performance of SR-KR, free bending test was carried out first. Fixing one end of SR-KR and inflating the air chamber at one side, we can get the results as shown in Fig. 8a and b. The maximum bending angle of SR-KR is 92.5°. The minimum working pressure reaching the maximum bending angle is 140 kPa. The first derivative of bending angle increases first and then decreases with the increase of working pressure. This phenomenon is in accordance with the derivation in (14).

From the free bending test, it can be seen that SR-KR meets the bending angle requirements mentioned in Section 2.

5.2. Mechanical property test

The mechanical property test is based on the torque test platform shown in Fig. 8d. This test is divided into two groups: constant bending angle and constant working pressure. According to the pre-inflation test, the safe working pressure range of SR-KR is 0–400 kPa. This test is performed within this pressure range.

Constant bending angle: The results are shown in Fig. 8c. With constant bending angle, the output torque of SR-KR is approximately linear with the working pressure, which is consistent with the derivation of (14). The proportion coefficient will decrease slightly with the increase of the bending angle. This phenomenon may be caused by slight changes in the cross-section of SR-KR at different bending angles.

Constant working pressure: The results are shown in Fig. 8e. The output torque and bending angle of the SR-KR are approximately in a negative linear relationship, and the proportion coefficient almost does not change with the working pressure.

Combining these two sets of experimental data, the relational surface for bending angle, working pressure, and output torque of the SR-KR can be obtained, as shown in Fig. 8f. It can be noted that SR-KR can provide larger output torque at smaller bending angle and higher working pressure.

From the relational surface, we can see that within the bending angle range in human gait range ($\leq 56.7°$), SR-KR can provide more than 26.3 Nm torque for user's knee joint with the working pressure in $0 \sim 400$ kPa. In addition, SR-KR can provide at most 34.1 Nm torque with 400 kPa working pressure.

Therefore, SR-KR meets the two functional requirements in Section 2 and has ability to assist human walking movements.

It should be noted that the parameters of the prototype are not the upper limit of SR-KR performance. Based on the modeling analysis and parameter design, we know that the mechanical properties of SR-KR can be further improved by increasing the sectional area of soft chamber and changing fabrication materials. For burly users, the size of the SR-KR can be enlarged to obtain greater output torque.

5.3. Trajectory-driven test

In order to verify the controllability and stability of the control system, trajectory-driven test was conducted. Considering the impact of knee joint injury on walking speed, this paper selects the 0.2 m/s gait trajectory as the test trajectory. Of course, users can adjust the speed or change to another motion trajectories according to their own needs, such as simple bending-stretching motion.

The test result is shown in Fig. 9. During the test, the maximum error of the whole process is 3.7°, which occurs when the bending angle tends to the regional extreme value. The average error is 1.18°. The
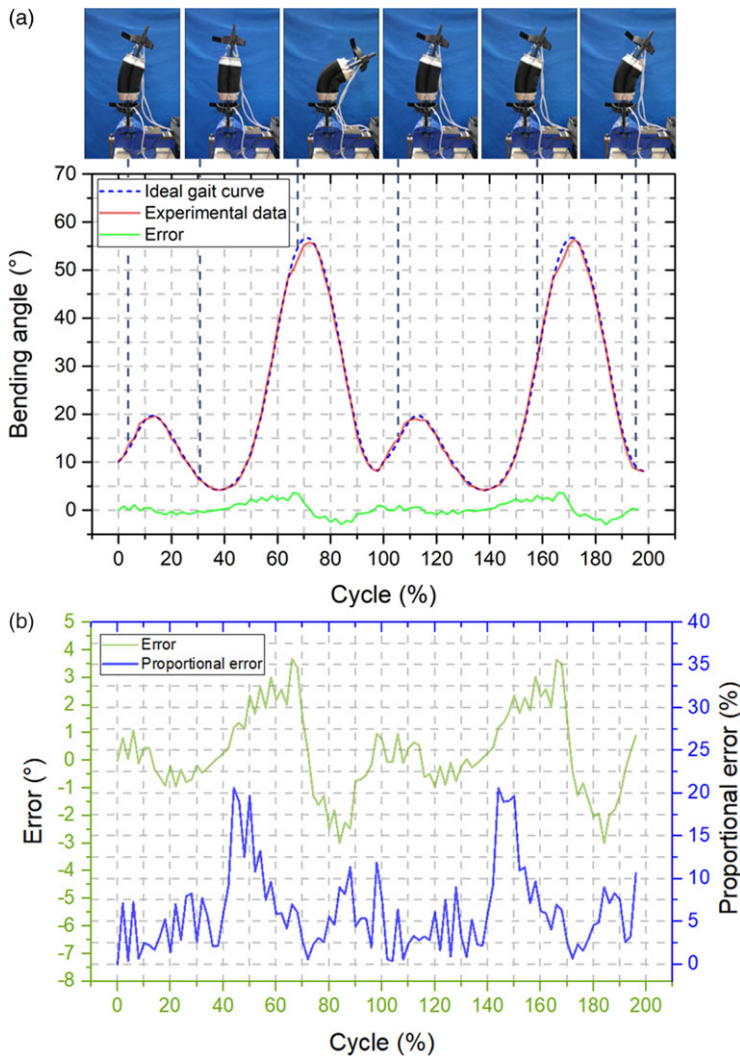
Figure 9. *Track driven test. (a) Comparison of actual and ideal trajectories of SR-KR. (b) Tracking error in test.*

maximum proportional error is 20.59%, and the average proportional error is 6.19%. Macroscopically, there is a delay of about 0.1 s between the actual and ideal motion. The response speed of the system is the main reason for the error.

On the whole, the overall motion trajectory of SR-KR is basically consistent with the ideal trajectory, though there are some errors. This result also shows that SR-KR has good controllability and stability under the control system above.

5.4. Lower limb wearing test

In order to verify the wearing effect of SR-KR, lower limb wearing test was conducted. Two surface electromyography (sEMG) sensors (SEN0240, DFROBOT, china) are placed at the vastus lateralis (VL) and vastus medial (VM). The subject walked with or without wearing SR-KR. The results of the middle four gait cycles in the test are shown in Fig. 10.

(a)

(b)
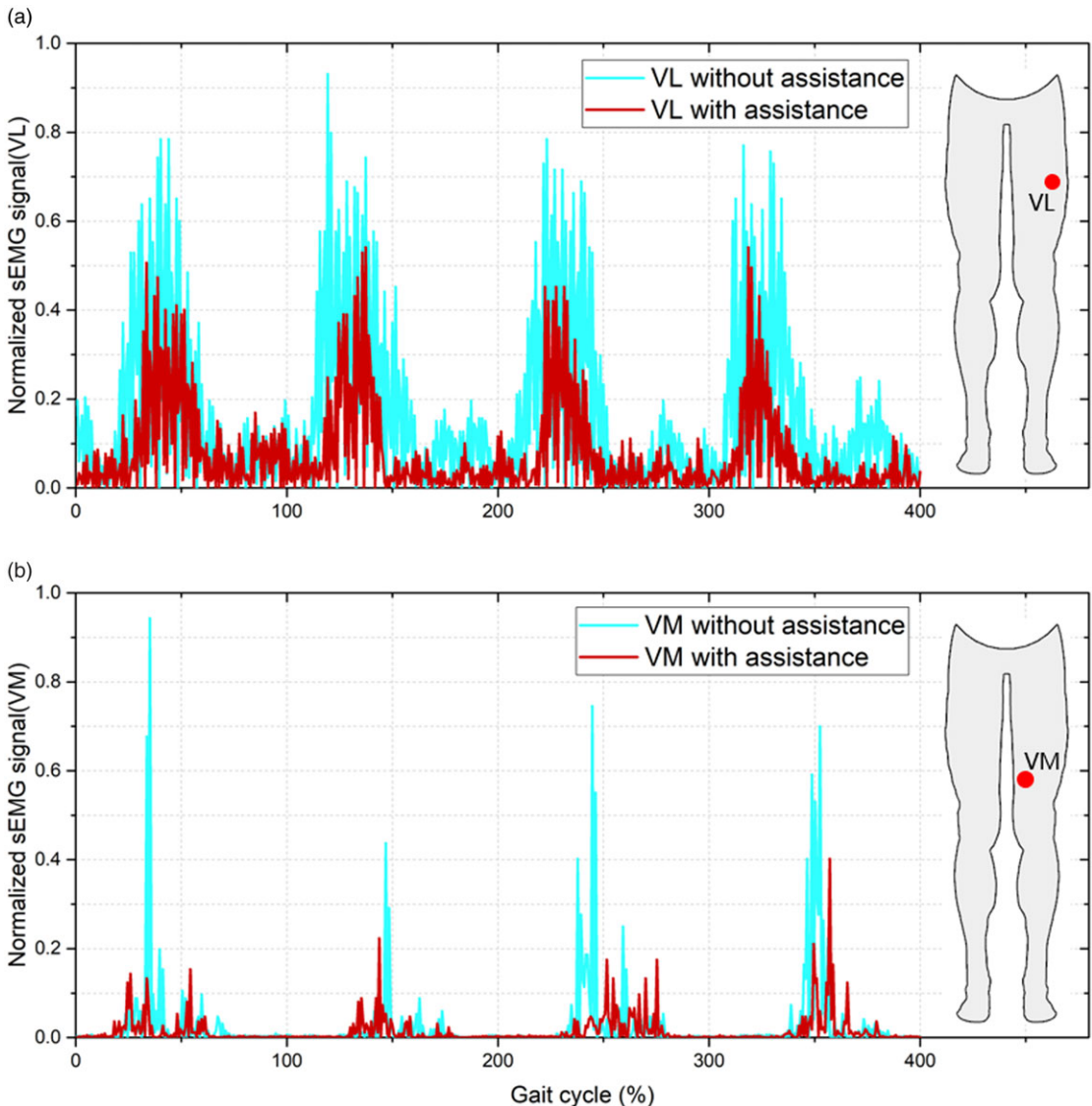
Figure 10. *Lower limb wearing test. (a) VL test result. (b) VM test result.*

It can be noted that after wearing SR-KR, the sEMG signal intensity at the VL and VM of the subject significantly decreased. The average sEMG signal intensity at VL decreased by 53.2%, and the peak value decreased by 41.9%. The average sEMG signal intensity at VM decreased by 49.1%, and the peak value decreased by 57.4%. Subject feels that the SR-KR suits well with the human lower limb and can provide objective torque support for the knee joint.

This indicates that wearing SR-KR can reduce the muscle burden during walking, demonstrating the effectiveness of SR-KR wearing. Furthermore, SR-KR has potential application value in the field of rehabilitation and human enhancement.

6. Conclusion

In this work, we completed the design, modeling, and control of a novel soft-rigid knee joint robot (SR-KR) for assisting motion. The main contributions of this work include:

1. A novel soft-rigid knee joint robot (SR-KR) for assisting motion is proposed based on the ergonomic functional requirements. SR-KR is worn on the parallel side of the knee joint and can provide more than 26.3 Nm torque for user's knee joint in human gait range with the working pressure in $0 \sim 400$ kPa and provide at most 34.1 Nm torque with 400 kPa working pressure.

2. The bending deformation mathematical model of SR-KR is established, which reveal the relationship among SR-KR's bending curvature, working pressure, and output torque.

3. A double closed loop servo control system is constructed to better apply SR-KR. In this system, each output of SR-KR is double detected by attitude servo and pressure servo to ensure the safe use of SR-KR.

SR-KR has great application potential in the field of human enhancement and rehabilitation, although there are still some engineering and technical problems to be solved.

In the future work, we will further improve the structure and control method of SR-KR, and promote it to hip and upper limb assisting motion.

Author contributions. Yinan Li designed the structure of SR-KR, derived the mathematical theoretical model of SR-KR, and built the control system.

Yuxuan Wang conducted experimental platform construction.

Shaoke Yuan performed the data analyses.

Yanqiong Fei helped perform the analysis with constructive discussions.

Competing interests. The authors declare no competing interests exist.

Ethical approval. Not applicable.

References

[1] Pł Maciejasz, Jörg Eschweiler, K. Gerlach-Hahn, A. Jansen-Troy and S. Leonhardt, "A survey on robotic devices for upper limb rehabilitation," *J. NeuroEng. Rehabil.* **11**(1), 3 (2014). doi: 10.1186/1743-0003-11-3.

[2] M. P. de Looze, T. Bosch, F. Krause, K. S. Stadler and L. W. O'Sullivan, "Exoskeletons for industrial application and their potential effects on physical work load," *Ergonomics* **59**(5), 671–681 (2016). doi: 10.1080/00140139.2015.1081988.

[3] A. J. Veale, K. Staman and H. van der Kooij, "Soft, wearable, and pleated pneumatic interference actuator provides knee extension torque for sit-to-stand," *Soft Robot.* **8**(1), 28–43 (2021). doi: 10.1089/soro.2019.0076.

[4] J. L. Pons, *Wearable Robot Technologies* (John Wiley & Sons, Ltd, New York, 2008) pp. 1–14.

[5] K. A. Major, Z. Z. Major, G. Carbone, A. Pîslă, C. Vaida, B. Gherman and D. L. Pîslă, "Ranges of motion as basis for robot-assisted poststroke," *HVM Bioflux* **8**(4), 192–196 (2016).

[6] B. G. Ariel, "Biomechanical Analysis of the Knee Joint During Deep Knee Bends with Heavy Load," **In:** *Biomechanics IV. International Series on Sport Sciences* (R. C. Nelson and C. A. Morehouse, eds.) (Palgrave, London, 1974) p. 44.

[7] S. Masiero, M. Armani and G. Rosati, "Upper-limb robot-assisted therapy in rehabilitation of acute stroke patients: Focused review and results of new randomized controlled trial," *J. Rehabil. Res. Dev.* **48**(4), 355–366 (2011). doi: 10.1682/jrrd.2010.04.0063.

[8] P. Polygerinos, Z. Wang, K. C. Galloway, R. J. Wood and C. J. Walsh, "Soft robotic glove for combined assistance and at-home rehabilitation," *Robot Auton. Syst.* **73**, 135–143 (2015). doi: 10.1016/j.robot.2014.08.014.

[9] G. Redlarski, K. Blecharz, M. Daxbkowski, A. Pałkowski and P. M. Tojza, Comparative analysis of exoskeletal actuators. *Pomiary Automat. Robot.* **16**, 133–138 (2012)

[10] A. Schiele, "Ergonomics of Exoskeletons: Objective Performance Metrics," **In:** *World Haptics-Third Joint Eurohaptics Conference & Symposium on Haptic Interfaces for Virtual Environment & Teleoperator Systems* (IEEE, 2009).

[11] H. Kazerooni, "A Review of the Exoskeleton and Human Augmentation Technology," **In:** *ASME Dynamic Systems & Control Conference* (2008).

[12] L. Fang, W. Cheng and Q. Wu, "Research on human exoskeleton based on rigid-flexible coupling system," *Mech. Sci. Technol. Aerosp. Eng.* **32**(5), 688–692 (2013).

[13] A. Schiele, "Ergonomics of Exoskeletons: Objective Performance Metrics," **In:** *World Haptics 2009—Third Joint EuroHaptics Conference and Symposium on Haptic Interfaces for Virtual Environment and Teleoperator Systems*, Salt Lake City, UT (2009) pp. 103–110.

[14] R. C. Browning, J. R. Modica, R. Kram and Goswami A., "The effects of adding mass to the legs on the energetics and biomechanics of walking," *Med. Sci. Sports Exerc.* **39**(3), 515–525 (2007).

[15] B. K. Dinh, M. Xiloyannis, C. W. Antuvan, L. Cappello and L. Masia, "Hierarchical cascade controller for assistance modulation in a soft wearable arm exoskeleton," *IEEE Robot. Autom. Lett.* **2**(3), 1786–1793 (2017). doi: 10.1109/LRA.2017.2668473.

[16] P. Polygerinos, N. Correll, S. A. Morin, B. Mosadegh, C. D. Onal, K. Petersen, M. Cianchetti, M. T. Tolley and R. F. Shepherd, "Soft robotics: Review of fluid-driven intrinsically soft devices; manufacturing, sensing, control, and applications in human-robot interaction," *Adv. Eng. Mater.* **19**(12), 1700016 (2017).

[17] G. Agarwal, N. Besuchet, B. Audergon and J. Paik, "Stretchable materials for robust soft actuators towards assistive wearable devices," *Sci. Rep.* **6**(1), 34224 (2016).

[18] A. T. Asbeck, S. M. M. De Rossi, K. G. Holt and C. J. Walsh, "A biologically inspired soft exosuit for walking assistance," *Int. J. Robot. Res.* **34**(6), 741–765 (2015).

[19] A. F. Hassanin, D. Steve and N. M. Samia, "A Novel, Soft, Bending Actuator for Use in Power Assist and Rehabilitation Exoskeletons," **In:** *IEEE International Conference on Intelligent Robots and Systems*, Vancouver, BC, Canada (2017) pp. 533–538.

[20] C. Dorin, C. Enrique, M. Luis and B. Dolores, "New design of a soft robotics wearable elbow exoskeleton based on shape memory alloy wire actuators," *Appl. Bionics. & Biomechan.* **2017**, 1–11 (2017). doi: 10.1155/2017/1605101.

[21] P. Polygerinos, Z. Wang, K. C. Galloway, R. J. Wood and C. J. Walsh, "Soft robotic glove for combined assistance and at-home rehabilitation," *Robot. Auton. Syst.* **73**(C), 135–143 (2014).

[22] L. N. Awad, J. Bae, K. O'Donnell, S. M. M. De Rossi, K. Hendron, L. H. Sloot, P. Kudzia, S. Allen, K. G. Holt, T. D. Ellis and C. J. Walsh, "A soft robotic exosuit improves walking in patients after stroke," *Sci. Transl. Med.* **9**(400), eaai9084 (2017). doi: 10.1126/scitranslmed.aai9084.

[23] C. M. Thalman, Q. P. Lam, P. H. Nguyen, S. Sridar and P. Polygerinos, "A Novel Soft Elbow Exosuit to Supplement Bicep Lifting Capacity," **In:** *2018 IEEE/RSJ International Conference on Intelligent Robots and Systems (IROS)*, Madrid, Spain (2018) pp. 6965–6971. doi: 10.1109/IROS.2018.8594403.

[24] J. Fang, J. Yuan, M. Wang, L. Xiao, J. Yang, Z. Lin, P. Xu and L. Hou, "Novel accordion-inspired foldable pneumatic actuators for knee assistive devices," *Soft Robot.* **7**(1), 95–108 (2020). doi: 10.1089/soro.2018.0155.

[25] S. Sridar, P. H. Nguyen, M. Zhu, Q. P. Lam and P. Polygerinos, "Development of a Soft-Inflatable Exosuit for Knee Rehabilitation," **In:** *2017 IEEE/RSJ International Conference on Intelligent Robots and Systems (IROS)*, Vancouver, BC, Canada (2017) pp. 3722–3727. doi: 10.1109/IROS.2017.8206220.

[26] C. T. O'Neill, C. M. McCann, C. J. Hohimer, K. Bertoldi and C. J. Walsh, "Unfolding textile-based pneumatic actuators for wearable applications," *Soft Robot.* **9**(1), 163–172 (2022). doi: 10.1089/soro.2020.0064.

[27] J. Wang, Y. Fei and W. Chen, "Integration, sensing, and control of a modular soft-rigid pneumatic lower limb exoskeleton," *Soft Robot.* **7**(2), 140–154 (2020). doi: 10.1089/soro.2019.0023.

[28] W. C. Huang, M. Feng, D. Z. Yang and G. Y. Gu, "Low-resistance, high-force, and large-ROM fabric-based soft elbow exosuits with adaptive mechanism and composite bellows," *Sci. China Technol. Sci.* **66**(1), 24–32 (2023). doi: 10.1007/s11431-022-2233-3.

[29] J. Chung, R. Heimgartner, C. T. O'Neill, N. S. Phipps and C. J. Walsh, "ExoBoot, a Soft Inflatable Robotic Boot to Assist Ankle During Walking: Design, Characterization and Preliminary Tests," **In:** *2018 7th IEEE International Conference on Biomedical Robotics and Biomechatronics (Biorob)*, Enschede, Netherlands (2018) pp. 509–516. doi: 10.1109/BIOROB.2018.8487903.

[30] I. M. Hasan, E. Q. Yumbla and W. Zhang, "Development of a Soft Inflatable Exosuit for Knee Flexion Assistance," **In:** *2022 9th IEEE RAS/EMBS International Conference for Biomedical Robotics and Biomechatronics (BioRob)*, Seoul, Republic of Korea (2022) pp. 1–6. doi: 10.1109/BioRob52689.2022.9925474.

[31] M. P. Kadaba, H. K. Ramakrishnan, M. E. Wootten, J. Gainey, G. Gorton and G. V. Cochran, "Repeatability of kinematic, kinetic, and electromyographic data in normal adult gait," *J. Orthop. Res.* **7**(6), 849–860 (1989). doi: 10.1002/jor.1100070611.

[32] T. Nagura, C. O. Dyrby, E. J. Alexander and T. P. Andriacchi, "Mechanical loads at the knee joint during deep flexion," *J. Orthop. Res.* **20**(4), 881–886 (2002).

[33] A. Nordez, P. Casari and C. Cornu, "Accuracy of Biodex system 3 pro computerized dynamometer in passive mode," *Med. Eng. Phys.* **30**(7), 880–887 (2008). doi: 10.1016/j.medengphy.2007.11.001.

[34] Y. Yang, Y. Chen, Y. Li, Z. Wang and Y. Li, "Novel variable-stiffness robotic fingers with built-in position feedback," *Soft Robot.* **4**(4), 338–352 (2017). doi: 10.1089/soro.2016.0060.

[35] D. Tedaldi, A. Pretto and E. Menegatti, "A Robust and Easy to Implement Method for IMU Calibration without External Equipments," **In:** *2014 IEEE International Conference on Robotics and Automation (ICRA)* (2014) pp. 3042–3049. doi: 10.1109/ICRA.2014.6907297.